Synthetic and Systems Biotechnology 9 (2024) 522–530

Contents lists available at ScienceDirect

Synthetic and Systems Biotechnology

journal homepage: www.keaipublishing.com/en/journals/synthetic-and-systems-biotechnology

Original Research Article

Filamentous morphology engineering of bacteria by iron metabolism modulation through MagR expression

Mengke Wei [a,b], Chenyang Han [a,b], Xiujuan Zhou [b,c], Tianyang Tong [b,d], Jing Zhang [b,c], Xinmiao Ji [b], Peng Zhang [b,c], Yanqi Zhang [b,c], Yan Liu [b,d], Xin Zhang [a,b,c], Tiantian Cai [b,c,e,**], Can Xie [b,c,e,*]

[a] Institutes of Physical Science and Information Technology, Anhui University, Hefei, Anhui, 230039, China
[b] High Magnetic Field Laboratory, Hefei Institutes of Physical Science, Chinese Academy of Sciences, Science Island, Hefei, Anhui, 230031, China
[c] Science Island Branch of Graduate School, University of Science and Technology of China, Hefei, Anhui, 230036, China
[d] Department of Anatomy, Anhui Medical University, Hefei, Anhui, 230032, China
[e] Institute of Quantum Sensing, Zhejiang University, Hangzhou, Zhejiang, 310027, China

ARTICLE INFO

Keywords:
Morphology regulation
Iron accumulation
Filamentous bacteria
MagR overexpression

ABSTRACT

The morphology is the consequence of evolution and adaptation. *Escherichia coli* is rod-shaped bacillus with regular dimension of about 1.5 μm long and 0.5 μm wide. Many shape-related genes have been identified and used in morphology engineering of this bacteria. However, little is known about if specific metabolism and metal irons could modulate bacteria morphology. Here in this study, we discovered filamentous shape change of *E. coli* cells overexpressing pigeon MagR, a putative magnetoreceptor and extremely conserved iron-sulfur protein. Comparative transcriptomic analysis strongly suggested that the iron metabolism change and iron accumulation due to the overproduction of MagR was the key to the morphological change. This model was further validated, and filamentous morphological change was also achieved by supplement *E. coli* cells with iron in culture medium or by increase the iron uptake genes such as entB and fepA. Our study extended our understanding of morphology regulation of bacteria, and may also serves as a prototype of morphology engineering by modulating the iron metabolism.

1. Introduction

Bacteria have adapted their shape to suit their particular environments and lifestyles. In general, bacteria can be classified according to three major basic shapes: Coccus, Bacillus, and Spiral. The bacterium *Escherichia coli* (*E. coli*) is a gram-negative rod-shaped bacillus with regular dimensions of about 1.5 μm long and 0.5 μm wide [1]. It has been extensively studied and become one of the standard model systems in biology. The morphology of bacteria is one of the critical features and is genetically determined, but could be changed either through genetic modification or expose to physical, chemical, and biological factors in the environment [2]. The manipulation of cell morphology through genetic modification or called morphology engineering have huge benefits to accelerate growth, reach higher cell density, simplify downstream separation and increase protein yield, thus has potential applications in bio-production [3]. Many shape related genes have been genetically modified to engineering cell morphology from bars to spheres [4,5], or bars to fibers [6]. However, little is known about the specific factors that determine why bacteria are shaped in a particular way and if we could conduct morphology engineering by modulating a specific metabolism pathway?

Exploring the bacteria morphology is crucial to understand the origin of life, as it globally restricts physical and chemical features of a cell. Life on earth developed in equilibrium with the hydrosphere and the lithosphere, taking from these all the elements necessary for performing essential functions [7]. As a consequence, a variety of metal ions are required for optimal functioning of living organisms during evolution [8,9]. Metals contribute to the proper folding and stability of biomacromolecules, and confer various biological functions [10,11]. Metalloproteins are at the heart of numerous biological processes ranging

Peer review under responsibility of KeAi Communications Co., Ltd.
* Corresponding author. High Magnetic Field Laboratory, Hefei Institutes of Physical Science, Chinese Academy of Sciences, Science Island, Hefei, 230031, China.
** Corresponding author. High Magnetic Field Laboratory, Hefei Institutes of Physical Science, Chinese Academy of Sciences, Science Island, Hefei, 230031, China.
E-mail addresses: tiantiancai@pku.edu.cn (T. Cai), canxie@zju.edu.cn (C. Xie).

https://doi.org/10.1016/j.synbio.2024.04.009
Received 14 January 2024; Received in revised form 16 March 2024; Accepted 8 April 2024
Available online 15 April 2024

from photosynthesis and respiration to natural product biosynthesis [12,13].

Among all the metals, iron is the fourth most abundant metal in the earth's crust [14], and is also a critical nutrient for the growth and survival of animals, plants and almost all microorganisms. It is widely used in various redox processes in e.g. asoxygen metabolism, electron transfer and DNA biosynthesis [15], and so on. Iron is also essential for the formation of biofilm, which regulates surface movement and stabilizes polysaccharide matrix [16,17]. The iron deficiency has a great effect on bacteria, and thus iron deprivation is an efficient way to limit bacterial growth.

The biological functionality of iron is almost entirely dependent upon its incorporation into proteins, either as a mono- or binuclear species, or in a more complex form as part of iron-sulfur clusters or haem groups [18]. A large proportion of internalized iron is housed within inorganic prosthetic groups called iron-sulfur clusters [19]. Iron-sulfur cluster is one of the oldest substances and exists widely in living organisms. The most common types of iron-sulfur clusters are rhombic [2Fe-2S], cubic [3Fe-4S] and cubic [4Fe-4S] [20]. These clusters confer a number of functions [21], like electron transfer, catalysis and regulatory processes [22]. Due to the mid-range redox potential of iron-sulfur clusters, they are commonly found as an electron transfer cofactor in various proteins, as well as in electron transport chains or pathways within a variety of redox enzymes [22].

In addition, Qin et al. in 2015 reported an iron-sulfur protein MagR (originally named IscA) played key roles in animal magnetoreception through the interaction with cryptochrome (Cry) [23]. MagR forms rod-like complex with Cry and showed intrinsic magnetic moment [23–26]. The iron-sulfur cluster of MagR has also been suggested to mediate the long range intermolecular electron transport chain in MagR/Cry complex [23,27–29], which implies the electron transfer may play essential roles in animal magnetoreception as well.

In the process of recombinant expression and purification of pigeon MagR, we noticed the morphological change of *E. coli* from rod-shaped to filamentous shape. A number of genetic and environmental factors which reshape the morphology of bacteria have been extensively studied previously, but how iron-sulfur protein affect the bacteria morphology has not been revealed. To address the underlying mechanism of how MagR expression induce the filamentous morphological change of *E. coli* and if this morphological change can be modulated by external magnetic field, here we systematically studied the effects of MagR expression on cell morphology and analyzed the change of metabolism and transcriptome of *E. coli* upon MagR recombinant expression. We found that the accumulation of iron content inside cells by over-expression of MagR directly led to filamentous morphological change of *E. coli*. Various experiments have been designed to increase the cellular iron content and the results further validate that iron content accumulation is the key to bacteria filamentation. The data we presented here not only elucidated a mechanism of bacteria filamentous morphology regulation which has not been revealed previously, but also suggested a potential strategy of bacteria morphology engineering by iron metabolism modulation through MagR expression.

2. Materials and methods

2.1. Bacterial strains and culture conditions

All cellular experiments were completed in *E. coli* BL21 (DE3) cells. For *E. coli* cells overexpressing wild type pigeon MagR (clMagR^{WT}), its homology *E. coli* IscA (ecIscA) or its loss-of-function mutant (clMagR^{3M}), or FepA, or EntB, or none (transfected with empty vector): cells were grown to OD600 0.5-0.6 at 37°C in LB medium with 50 mg L^{-1} Kanamycin and the protein expression was induced with 20 μM isopropyl-β-D-1-thiogalactopyranoside (IPTG) at 15°C overnight. For magnetic field treatment during cell culture: *E. coli* cells were cultured in LB medium and placed on neodymium iron boron (NdFeB) N38 permanent magnets (length × width × height: 10 × 10 × 2 cm, Hefei Gaoshu Magnetic Materials, Hefei, China). The magnetic intensity was measured as 0.5 T on the surface of NdFeB permanent magnets. Non-magnetic aluminum 6061 (Al 6061) alloy block of the same size was used as a sham control of the magnet (Hefei Gaoshu Magnetic Materials, Hefei, China).

2.2. Fluorescence imaging

E. coli cells overexpressing ecIscA, clMagR^{WT} and none (transfected with empty vector) were stained with 20 μg mL^{-1} FM4-64 (Invitrogen, USA) and 20 μg mL^{-1} Hoechst 33258 (Beyotime Institute of Biotechnology, Jiangsu, China) for 3 min on ice and room temperature for 20 min. The mixtures were then centrifuged at 12000 rpm for 1 min and cells remove the supernatant and retain 5 μL of dye for preparation. All the images were taken with a confocal microscope (Olympus, Tokyo, Japan).

2.3. LIVE/DEAD bacteria staining

To monitor the viability of bacterial populations, LIVE & DEAD bacterial staining kit was purchased from Yeasen Biotechnology (Shanghai, China) and stained bacterial according to the manufacturer's protocol. Briefly, one volume of DMAO and two volumes of EthD-III were mixed in a microcentrifuge tube, and after full mixing, 8 vol of 0.85% NaCl solution were added to obtain a 100 × dye solution. 1 μL of 100 × dye solution was added 100 μL of bacterial suspension. Then, cells were stained at room temperature in dark for 15 min. The images were photographed by a confocal microscope (Olympus SpinSR10, Tokyo, Japan).

2.4. Counting of cells with filamentous morphology

Images of cells expressing clMagR^{WT}, clMagR^{3M}, ecIscA, FepA, EntB, or none (transfected with empty vector), were randomly selected and the lengths of each cell were measured using the length measurement tool in cellSens (Olympus, Tokyo, Japan). Elongated *E. coli* cells were defined as cells with length reached equal or above 5 μm (corresponding to roughly 2-3 folds of the length of a regular rod-like *E. coli*), and filamentous cells were defined as cells with length reached equal or above 15 μm (corresponding to roughly 7-8 folds of the length of a regular rod-like *E. coli*). The percentage of elongated cells were calculated by counting the number of elongated cells in every 100 cells and for each experiment, at least 500 cells were counted. We also used the term "the number of filamentous cells" to describe the numbers of filamentous cells (length equal or above 15 μm) in every 500 cells to show those extremely long cells which would almost never be observed in normal conditions.

2.5. Comparative transcriptomic analysis

To further investigate the possible molecular mechanism of the morphological change of *E. coli* cells upon clMagR^{WT} over-expression, a comparative analysis of the gene expression profiles was performed. We sequenced and compared the transcriptome of *E. coli* cells with or without clMagR^{WT} recombinant expression. Total RNA from all samples including 3 independent RNA preparations derived from *E. coli* cells expressing clMagR^{WT} and 3 independent replicates from *E. coli* cells transformed with empty vector, were extracted and purified using the same protocol and reagents as reported by Chen et al. [30]. cDNA library construction was performed according to the protocol described by Chen et al. [30]. After completing library construction, the concentration and purity of the extracted RNA were detected by ND-2000 (NanoDrop Technologies, USA). The integrity of RNA was detected by agarose gel electrophoresis, and Agilent 2100 (Agilent Technologies, USA) were used to determine the RIN value. After passing library quality

inspection, the library preparations were sequenced on an Illumina platform, and paired-end reads were generated. Clean data (clean reads) were obtained from the screening of raw data (raw reads). The Q20, Q30, GC-content, and sequence duplication levels of the clean data were calculated and suggested that the quality of sequencing results was sufficiently high and reliable for the subsequent transcriptome analysis (Supplementary Table 1). Principal component analysis (PCA) was performed to verify the reliability of the repeated experiments.

To identify DEGs (differential expression genes) between two different treatments, the expression level of each gene was calculated according to the transcripts per million reads (TPM) method. RSEM [31] was used to quantify gene and isoform abundance. Essentially, differential expression analysis was performed using the DESeq2 with $|\log_2(\text{foldchange})| \geq 1$ and P-adjust ≤ 0.05. Functional enrichment analysis was performed to identify which DEGs were significantly enriched in GO terms and metabolic pathways at Bonferroni-corrected p-value ≤ 0.05 in comparison with the whole-transcriptome background. GO functional enrichment and KEGG pathway analysis were performed using Goatools and KOBAS [32], with adjusted $p < 0.05$ using the Benjamin-Hochberg method. Additionally, we performed an extensive literature survey for these genes to uncover their roles in filamentation of bacterial cells. DEGs from these genes were identified and their expression patterns were illustrated using the heatmap illustrator of TBtools [33].

2.6. Protein expression and purification

The expression vectors containing clMagR^{WT} or clMagR^{3M} genes were constructed as described previously [23]. clMagR^{3M} was obtained by mutating three conserved cysteine residues (C60/C124/C126) to alanine as reported previously [34]. The protein expression was induced with 20 μM IPTG at 15°C overnight, and bacteria cells were then harvested. The cell pellets were resuspended in lysis buffer (20 mM Tris, 500 mM NaCl, pH = 8.0) with complete protease inhibitor cocktail and lysed by sonication on ice. After centrifugation, the supernatant was collected and loaded into Strep-Tactin affinity column (IBA, USA). The column was washed about 20 column volumes (CV) with washing buffer (20 mM Tris, 500 mM NaCl, pH = 8.0) to remove unbound proteins. After washing, proteins were eluted using elution buffer (20 mM Tris, 500 mM NaCl, 5 mM desthiobiotin, pH = 8.0) and the protein purity was verified by SDS-PAGE. For all SDS-PAGEs, protein Ladder (Thermo Scientific, Product# 26616) was used as the molecular weight standards.

2.7. Ferrozine assay

For iron content in purified protein measured by Ferrozine assay, followed the protocol as described before [24,26]. For intracellular iron content measured by Ferrozine assay: cells expressing clMagR^{WT}, clMagR^{3M}, ecIscA, EntB, FepA or none, were recovered by centrifugation (8000 rpm, 10 min), and then washed six times in ddH_2O to remove culture media and iron absorbed on the cell surfaces. The washed bacteria were dried to constant weight, and then weighed and digested with nitric acid until the solution was clarified.

Ferrous iron reacts with ferrozine (0.1% (w/v) ferrozine in 50% (w/v) ammonium acetate) to form an intense purple complex that can be quantified spectrophotometrically at 562 nm using a microplate reader. A series of ferric chloride ($FeCl_3$) solutions (0.1–1 mM) were prepared in HCl (1 M) to generate a standard curve. The iron content in purified proteins, or in cell samples after pretreatment as described above were quantified and analyzed by Ferrozine assay based on the stand curve. Briefly, aliquots of protein (or cell samples) and HAHCl mixture (80 μL HAHCl and 20 μL proteins (or cell samples) at 100 μM, total 100 μL) were incubated at 37°C for 30 min in the dark in a 96-well plate, then, 100 μL ferrozine was added into each well and incubated at 37°C for additional 15 min in the dark. The iron ferrozine complex was measured at 562 nm on a microplate reader (Tecan Spark, Switzerland). Histogram and statistical analyses were performed by GraphPad Prism software. Protein and cell samples were tested for differences in total iron using a Student's t-test and were considered significantly different at $p < 0.05$.

2.8. Intracellular iron content analyses using in vivo electron paramagnetic resonance measurement

The cells expressing clMagR^{WT}, clMagR^{3M}, ecIscA, EntB, FepA or none, were harvested and resuspended in LB medium containing 20 mM deferoxamine and incubated at 37°C for anther 15 min as described by the *Imlay*'s group in 2002 [35]. Then, the cells were washed with 10 mM diethylenetriaminepentaacetic acid once, and 20 mM cold Tris-HCl (pH = 7.4) twice and resuspended in 20 mM cold Tris-HCl (pH = 7.4). 200 μL of the above samples were mixed with 50 μL of glycerol and transferred to an EPR tube (Wilmad 707-SQ-250 M, USA) and frozen in liquid nitrogen until EPR measurements. The EPR signals were monitored at different temperatures (10 K) with a microwave frequency of 9.40 GHz, a microwave power of 2 mW, a modulation amplitude of 2.0 G and a receive gain of 1.0×10^4.

2.9. Ultraviolet–visible absorption

Purified protein including clMagR^{WT}, clMagR^{3M} were prepared at 200 μM in TBS buffer (20 mM Tris, 150 mM NaCl, pH = 8.0) and UV-visible (UV-Vis) absorption were measured in the near UV-Vis wavelength (300–600 nm) and recorded using a spectrophotometer (Thermo Scientific, NanoDrop One^C, USA).

2.10. Statistical analysis

Quantitative data were obtained from at least three biological replicates. Origin 9 was used for histogram and statistical analysis. The data were all mean ± standard deviation. Student's t-test was used to examine the raw data. Differences were considered significant at * $p < 0.05$.

3. Result

3.1. The filamentous morphology of Escherichia coli upon MagR over-expression

Previously, we identified a highly conserved A type iron-sulfur protein MagR (originally named IscA1) as putative magnetoreceptor [23]. Recombinant expression and purification of animal MagR from *E. coli* (strain BL21) have become the major source for biophysical studies in the lab since then. While most of attentions have paid to the functions related to magnetoreception of the protein, we continuously noticed that the filamentous morphological change of bacteria upon MagR expression. Questions have been raised on why over-expression of an iron-sulfur protein could turn *E. coli* from rod to filament and may magnetic field affect this process? And if so, can we develop a morphology engineering approach based on this phenomenon? Thus, we decided to investigate the underlying mechanism.

Increased cell size (mostly the length of cell) has been observed in cells over-expressing clMagR compared with that of cells transformed with empty vector (Fig. 1). The lengths of each *E. coli* cell were measured. Considering most *E. coli* cells are rod-like shape with a length around 0.5-2 μm, 'elongated cells' were defined as cells with the length reached or above 5 μm and 'filamentous cells' were defined as those cells with length reached or above 15 μm in this study. Since filamentous cells were extremely rare to be observed under regular conditions, in this study, we calculated the ratio or percentage of elongated cells (Fig. 1A), and also counted the numbers of filamentous cells to give a full image of the morphology change of *E. coli* cells (Fig. 1B). Although the percentage of elongated cells were not very high (around 7-8%), the presence of elongated cells was consistent in every experiment and more

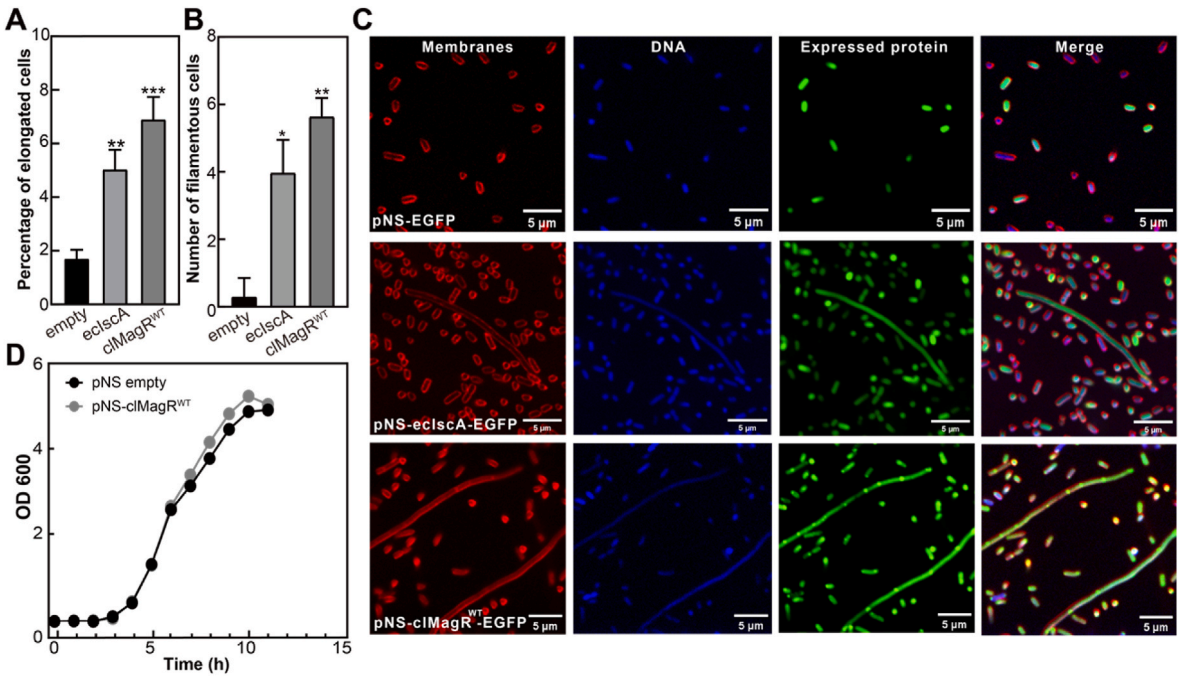

Fig. 1. Overproduction of clMagR or ecIscA both caused an increase in the proportion of filamentous cells in *E. coli* BL21 (DE3) strain. (**A,B**) Percentage of elongated cells (**A**) and Number of filamentous cells (**B**) in *E. coli* overexpressing ecIscA or clMagR^{WT}. (**C**) Confocal image of *E. coli* cells double stained with Hoechst 33258 (DNA) and FM4-64 (Membranes). Scale bars represent 5 μm. (**D**) Growth curves of *E. coli* cells overexpressing clMagR or none at 37°C.

importantly, the extremely long cells (termed as filamentous cells) were observed in every experiment. Thus, we believe that the morphology change of *E. coli* cells was consistent and could be the consequence of clMagR overexpression. To verify if over-production of other iron-sulfur proteins has similar effects, we compared the filamentous morphology formation in *E. coli* cells over-expressing its own IscA protein (ecIscA) as well (ecIscA, Fig. 1A). The results show that both ecIscA and clMagR overproduction led to the increase of the ratio of elongated cells and the filamentous morphology formation significantly.

To further validate the connection between phenotype of filamentous cell and overproduction of MagR/IscA protein, enhanced green fluorescent protein (EGFP) was used as fluorescent tag and fused to the C-terminal of clMagR and ecIscA to monitor the expression of clMagR and ecIscA in cells. Fluorescent dye FM4-64 and Hoechst 33258 were used to stain cell membrane and nucleic acid, respectively. Confocal microscopy images confirmed the expression of clMagR and ecIscA in most *E. coli* cells (Fig. 1C). It is worth noting that the expression of clMagR accumulated at intervals along the filamentous cells, probably at the putative division site, as revealed by the EGFP fluorescent. In contrast, the expression of ecIscA appeared to be evenly distributed in cells.

To validate the cell viability after clMagR and ecIscA overexpression, we performed LIVE/DEAD bacterial staining based on based on the membrane integrity of the cell. Briefly, bacteria were stained with DMAO (green) and EthD-III (red), and EthD-III remains excluded from bacteria with structurally intact cytoplasmic membranes. Therefore, it was typical that the viable bacterial population demonstrated strong green fluorescence; in addition, a completely dead population showed strong green and red fluorescence. The results showed that bacteria cells were healthy in all conditions, and cells overexpressing clMagR and ecIscA had similar viability as control cells (Supplementary figure S1). It is interesting to point out that most filamentous cells were alive, indicating the dramatical morphology change did not affect the cell viability.

It has been suggested that inhibition of cell division in *B. subtilis* could result in filamentous cells [36]. Thus, we measured the growth rate of *E. coli* cells over-expressing clMagR or none using OD600 curves to validate if the over-production of an exogenous gene caused a delay in cell division (Fig. 1D). The results showed similar growth rate between cells over-expressing clMagR and wild type cells, which is also consistent with the results of cell viability assay (Supplementary figure 1). Thus, overproduction of clMagR^{WT} or its homology ecIscA in *E. coli* BL21 (DE3) strain did not affect the growth rate of cells but both resulted in filamentous cell formation.

3.2. Comparative transcriptomic analysis of differentially expressed genes (DEGs)

To further investigate the underlying mechanism of morphological change of *E. coli* cells over-expressing clMagR, a comparative analysis of the gene expression profiles was performed. RNA preparations derived from 3 independent biological replicates of *E. coli* cells overexpressing clMagR^{WT} (named clMagR^{WT} group) and 3 from cells transfected with empty vectors (named empty group) as control were sequenced and compared.

An assessment of the relationships between biological replicates is essential for analyzing transcriptome sequencing data, PCA was thus performed to confirm the uniformity between biological replicates of the 2 sample groups. Three biological replicates from empty and clMagR^{WT} groups were clustered tightly and separated distinctly from each other, indicating the reliability of our RNA-seq results (Fig. 2A). The expression data of each gene were normalized using FPKM, and a total of 586 differentially expressed genes (DEGs) (212 upregulated and 374 down-regulated) were detected by the DESeq2 method with the threshold of adjusted p-value <0.05 and $|\log_2 (\text{fold change})| \geq 1$ (Fig. 2B).

Then, the DEGs were enriched in the gene ontology (GO) and kyoto encyclopedia of genes and genomes (KEGG) database. To identify the processes enriched in significant DEGs, we subjected significant DEGs to GO functional annotation and term enrichment analysis, a tool developed to represent common and basic biological information. In our study, GO enrichment analysis corresponding to 586 significant DEGs were produced and assigned to three categories. The 10 GO terms with the highest enrichment are shown in Fig. 2C. Among the top 10 GO terms, most of DEGs in the comparison of clMagR^{WT} vs. Empty were

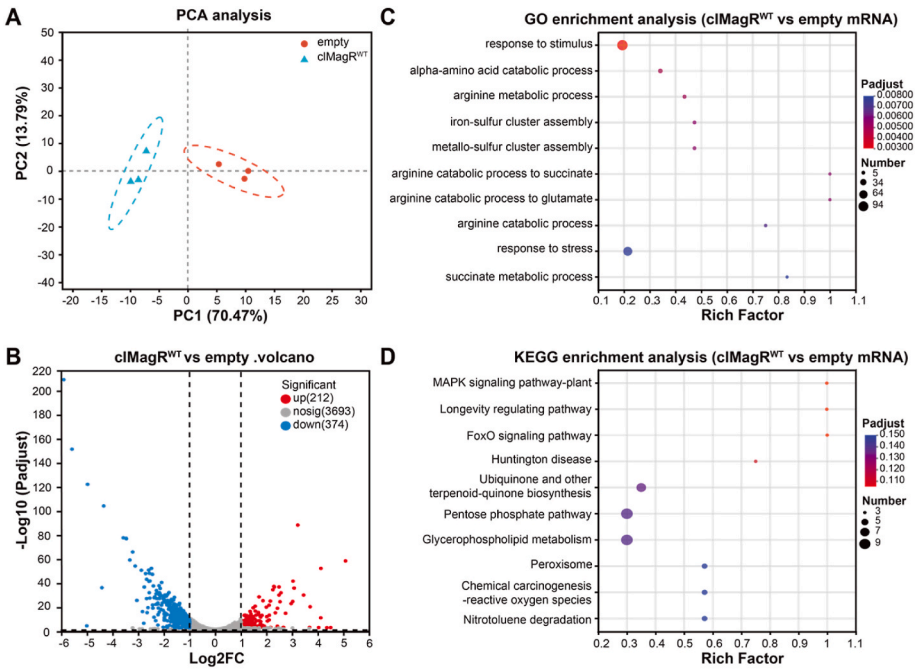

Fig. 2. Statistical analysis on RNA sequencing results. (A) PCA analysis. (B) Volcano plot of upregulated and downregulated DEGs of the overproduction of clMagR^{WT}. GO (C) annotations and KEGG (D) enrichment analysis of DEGs of *E. coli* cells upon MagR over-expression. Pathway enrichment analysis plots (top 10) of expressed metabolisms according to $p < 0.05$.

enriched in biological process (BP), such as "iron-sulfur cluster assembly", "metallo-sulfur cluster assembly" et al. Mapping these DEGs to the pathways from databases KEGG suggested that these genes are significantly clustered into several key signaling pathways, namely Huntington disease, Longevity regulating pathway, Pentose phosphate pathway and so on (Fig. 2D).

3.3. Cell division- and iron metabolism-related genes involved in morphological change

Several genes related in bacterial cell division including ftsL and zapA [37], have been identified significantly upregulated upon the overproduction of clMagR^{WT}, based on GO annotations and KEGG enrichment analysis (Fig. 3A). TPM was used to measure the expression level of these genes or transcripts, and the results is consistent with the morphological change observed in Fig. 1B.

Many genes related in metal ion iron metabolism including iron uptake, iron-sulfur cluster assembly, metallo-sulfur cluster assembly were significantly enriched as well in the functional enrichment analysis when cells overexpressing clMagR^{WT}. The expression patterns of the 9 genes which play essential roles in iron uptake and iron-sulfur cluster assembly were shown in response to the overproduction of clMagR^{WT} (Supplementary Figure 2).

Bacteria acquire iron through the secretion of siderophores, which are secondary metabolites that scavenge iron from environmental stocks and deliver it to cells via specific receptors [38]. During this process, both entB and entD are involved in the synthesis of siderophore, whereas fepA, exbB and exbD play roles in intracellular pumping of iron-siderophore complexes. Interestingly, all these genes showed significantly upregulated expression level as shown by TPM in cells overexpressing clMagR^{WT} (Fig. 3B).

The assembly of iron-sulfur clusters is mediated by complex machineries both in prokaryotes and eukaryotes. In bacteria, ISC machinery including key members such as IscA, IscU, IscS and IscR is considered the housekeeping system responsible for the maturation of a large variety of iron-sulfur proteins [39]. In agreement with Fig. 3B, all these genes in ISC machinery showed upregulated expression as well, as shown in Fig. 3C.

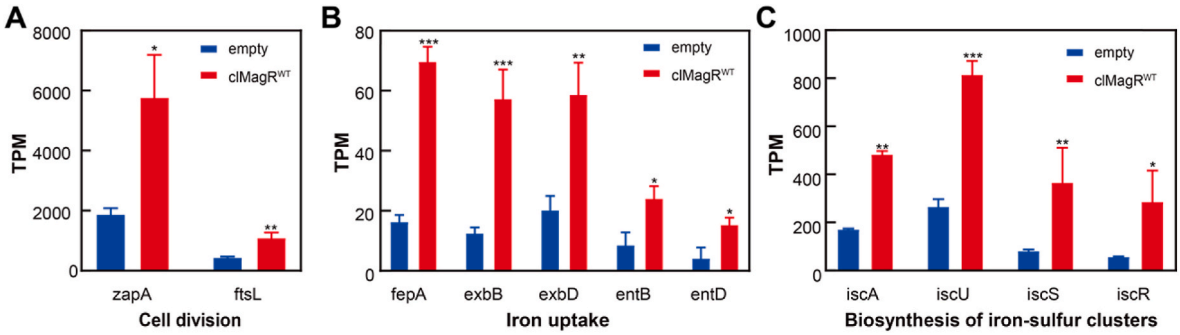

Fig. 3. Cell division- and Iron metabolism-related genes involved in morphological change of *E. coli* cells overexpressing clMagR^{WT}. (**A**) Cell division related genes zapA and ftsL showed upregulated expression upon the overexpression of clMagR, as shown by the TPM values. (**B**) Iron uptake related genes, fepA, exbB, exbD, entB and entD, were upregulated upon clMagR overproduction in *E. coli*, as shown by TPM values. (**C**) Genes involved in biosynthesis of iron-sulfur clusters including iscA, iscU, iscS and iscR were upregulated upon clMagR overproduction in *E. coli*, as shown by TPM values.

3.4. Iron accumulation may cause the filamentous morphological change

Comparative transcriptomic analysis of cells overexpressing clMagR^{WT} compared with control cells strongly suggested that the major differences are the change of iron metabolism and iron accumulation inside the cells. Thus, we measured the total iron content of *E. coli* BL21 (DE3) cells expressing none, ecIscA and clMagR^{WT} using Ferrozine assay, an accurate and rapid method of the quantitation of iron in biological systems [40–42]. The data clearly showed that cells overexpressing clMagR^{WT} and ecIscA, which exhibit filamentous shape as shown in Fig. 1AB, have higher iron content compared with control cells (Fig. 4A). And when cells overexpressing clMagR^{WT}, which should the highest ratio of filamentous shape changes, the total iron content inside of cells reached 2-3 folds higher than the control cells.

To further validate the results and to probe the intracellular iron content of *E. coli* cells, *in vivo* electron paramagnetic resonance (EPR) approach was applied. The method was developed by the *Imlay*'s group in 2002 [35]. Briefly, exponentially growing *E. coli* cells were treated with the membrane-permeable iron chelator desferrioxamine. The cells were then washed with the membrane-impermeable iron chelator diethylenetriaminepentaacetic acid to remove the extracellular free iron. Because the desferrioxamine-ferric iron complex has an EPR signal at g = 4.3. The amplitude of the EPR signal at g = 4.3 reflects the relative amount of the intracellular iron content inside the cells [43]. We compared the intracellular iron contents of cells overexpressing ecIscA, clMagR^{WT} and none, it is obvious that the overproduction of both proteins increased the intracellular iron content significantly, especially in cells overexpressing clMagR^{WT}, as shown by an increased amplitude of the EPR signal at g = 4.3 (Fig. 4B).

Taking together, overexpression of iron-sulfur proteins clMagR or its homology protein ec IscA induced filamentous morphological changes of the bacteria cells, and this morphological change was always accompanied by intracellular iron content increase. Thus, questions raised, would intracellular iron accumulation lead to the filamentous shape change of bacteria cells?

To validate this hypothesis, two sets of experiments were designed to test if similar filamentous morphological change could be obtained by manipulating the intracellular iron content of *E. coli* through either supplement exogenous iron into the culture medium or overexpressing of iron-transporters, instead of clMagR or ecIscA overproduction.

Firstly, intracellular iron content increase was achieved by supplementing the bacteria with ferric citrate in LB medium during culture. Different concentration of ferric citrate ranging from 10 μM to 1 mM were added into the LB medium, and after harvest the cells and washed out extracellular free iron, the iron content of *E. coli* cells was measured by Ferrozine assay (Fig. 4C), and further confirmed by *in vivo* EPR (Fig. 4D). The results showed that with the higher ferric citrate concentration added during culture, the higher intracellular iron content of *E. coli* cells was observed (Fig. 4CD). The morphology changes of bacteria occurred when exogenous iron was supplemented into the culture medium. The percentages of elongated cells were calculated (Fig. 4E) and the numbers of filamentous cells were counted (Fig. 4F). The percentage of elongated cells and the number of filamentous cells gradually increased along with the intracellular concentration of iron increased upon ferric citrated treatments. When 50 μM ferric citrate was added into the LB culture medium, the morphology change of bacteria reached the similar level as cells overexpressing ecIscA, and when ferric citrate concentration in culture medium reached 500 μM or 1 mM, the ratio further increased and reached similar level as cells overexpressing clMagR^{WT}.

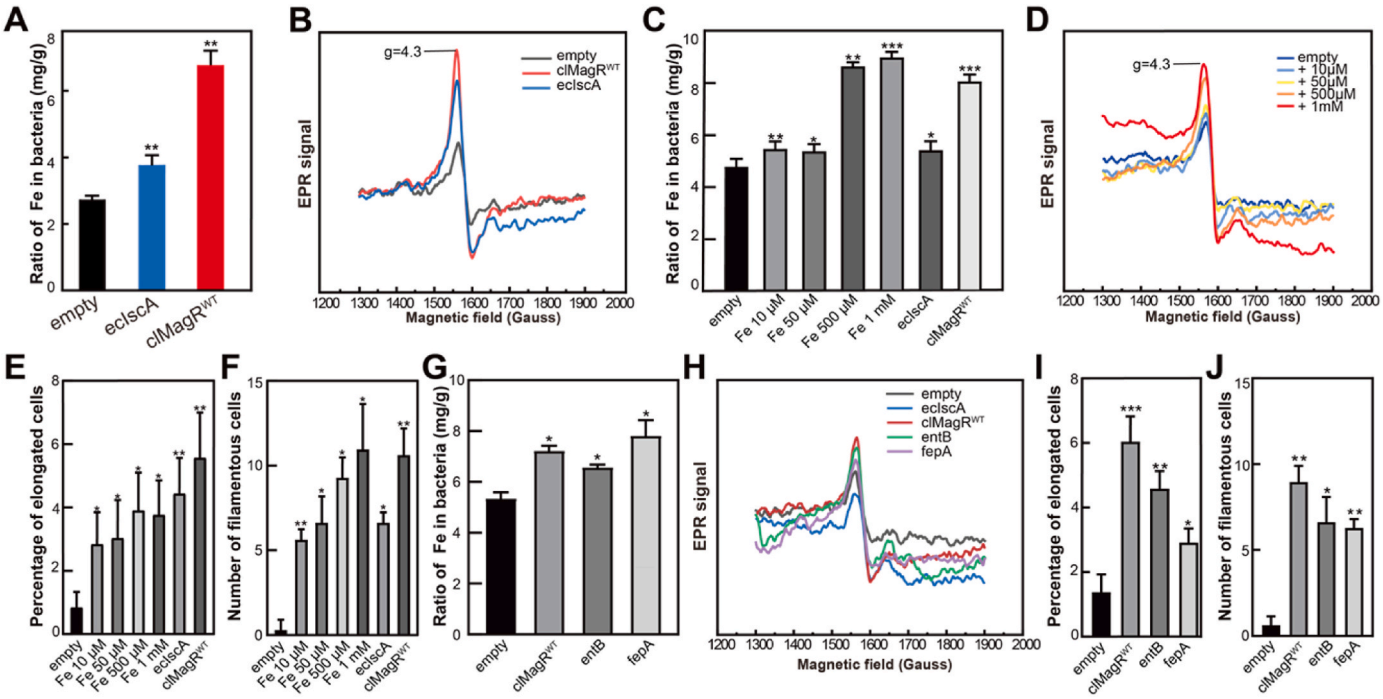

Fig. 4. Increased intracellular iron content caused filamentous morphological change in *E. coli* cells. (**A**) Iron content of cells overexpressing clMagR^{WT} (red), ecIscA (blue), and none (transfected with empty vector, black) measured by Ferrozine assay. Student's t-test: **, $p < 0.01$; ***, $p < 0.001$; ns, $p > 0.05$, "ns" indicate no significant differences. Error bars: SD of three independent replicates. (**B**) The EPR spectra of the *E. coli* cells treated with an iron indicator deferoxamine, as described text and methods. The amplitude of the EPR signal at g = 4.3 reflects the relative intracellular iron concentration in *E. coli* cells. (**C, D**) Intracellular iron content of cells cultured in LB supplemented with different concentration of ferric citrate measured by Ferrozine assay (**C**) and *in vivo* EPR (**D**). (**E, F**) Percentage of elongated cells (**E**) and the number of filamentous cells (**F**) in *E. coli* cultured in LB supplemented with different concentration of ferric citrate, compared with cells transfected with empty vector (empty) and cells overexpressing ecIscA and clMagR^{WT}. (**G, H**) Intracellular iron content of cells overexpressing iron uptake related genes, entB and fepA, measured by Ferrozine assay (**G**) and *in vivo* EPR (**H**). (**I, J**) Percentage of elongated cells (**I**) and the number of filamentous cells (**J**) in *E. coli* overexpressing iron uptake related genes, entB and fepA, compared with cells transfected with empty vector (empty) and cells over expressing clMagR^{WT}.

Secondly, *E. coli* iron uptake genes including entB and fepA were overexpressed in BL21 (DE3) cells separately, and the expression level of entB and fepA were confirmed by SDS-PAGE after IPTG induction (supplementary Figure 3). The intracellular iron contents of cells overexpressing entB or fepA measured by Ferrozine assay (Fig. 4G) and *in vivo* EPR (Fig. 4H) as described above. As expected, introducing high expression of both entB and fepA also lead to the iron accumulation inside of cells, thus significantly increased the intracellular iron content as well. Consistently, morphology analysis also showed increased percentage of elongated cells (Fig. 4I) and number of filamentous cells (Fig. 4J) along with the increased intracellular iron contents, though still lower than that caused by over-production of clMagR.

3.5. Blocking the function of clMagR rescued the morphological change caused by clMagR^{WT} overexpression

The data we presented above clearly suggested the increased percentage of filamentous cells of *E. coli* were accompanied by increased intracellular iron contents, no matter caused by over-expression of iron-sulfur protein clMagR^{WT} or ecIscA, or by iron uptake protein entB and fepA, or by supplement with ferric citrate in culture medium (Fig. 4).

To further validate this hypothesis, it is necessary to test if we specifically inhibit the function of clMagR by mutagenesis could rescue the morphological change caused by over-expression of clMagR. Removing the iron-sulfur cluster binding site of clMagR would certainly block the function of the protein as an iron-sulfur protein, and as a magnetoreceptor as well [24,34]. Therefore, cysteine-to-alanine substitution mutant clMagR^{3M} (C60A, C124A, and C126A mutation of clMagR^{WT}) has been made and overexpressed in *E. coli* BL21 (DE3) cells as described previously [34].

clMagR^{WT} and its loss-of-function mutant clMagR^{3M} were recombinantly expressed and purified as described [24,34], and UV-Vis absorption were measured (Fig. 5A). As expected, purified clMagR^{WT} showed absorption from 300-600 nm region, and with absorption peaks at 325 and 415 nm, and a shoulder at 470 nm (Fig. 5A, red line), whereas all these absorption peaks disappeared in clMagR^{3M} (Fig. 5A, gray line), indicating the cysteine-to-alanine substitution abolished iron-sulfur cluster binding in clMagR^{3M}. The iron content in purified proteins were measured by Ferrozine assay (Fig. 5B). clMagR^{3M} showed significantly decreased though not completely abolished iron content compared with clMagR^{WT}. It is possible that clMagR^{3M} retained the iron binding activity as reported previously [24]. Consistently, the clMagR^{WT} protein showed brown color and clMagR^{3M} appeared much light color in the solution (Fig. 5B).

After *E. coli* transformation, we determined the intracellular iron content of the cells overexpressing clMagR^{WT}, clMagR^{3M} and none (transformed with empty vector as control) using both Ferrozine assay (Fig. 5C) and *in vivo* EPR (Fig. 5D). The results show that the total intracellular iron content of cells expressing clMagR^{3M} is also reduced to comparable level with that of control cells (Fig. 5CD). Interestingly, by comparing the percentages of elongated cells (Fig. 5E) and the number of filamentous bacteria cells (Fig. 5F) in each group, we found that the morphology of *E. coli* cells overexpressing clMagR^{3M} have dropped to similar level as in control cells (labeled as empty), and much lower than those *E. coli* cells overexpressing clMagR^{WT}. MagR play essential roles not only as iron-sulfur cluster assembly protein, but also as magnetoreceptor in animals, thus, we also compared the magnetic field effect (MFE) on the morphology regulation of *E. coli* cells overexpressing clMagR^{WT} and its mutant clMagR^{3M} (Fig. 5EF). Cells overexpressing clMagR^{WT}, clMagR^{3M} and none were growing in the presence or absence of 0.5 T magnetic field, and filamentous cells were counted, and the percentage of elongated cells were calculated and compared. The data

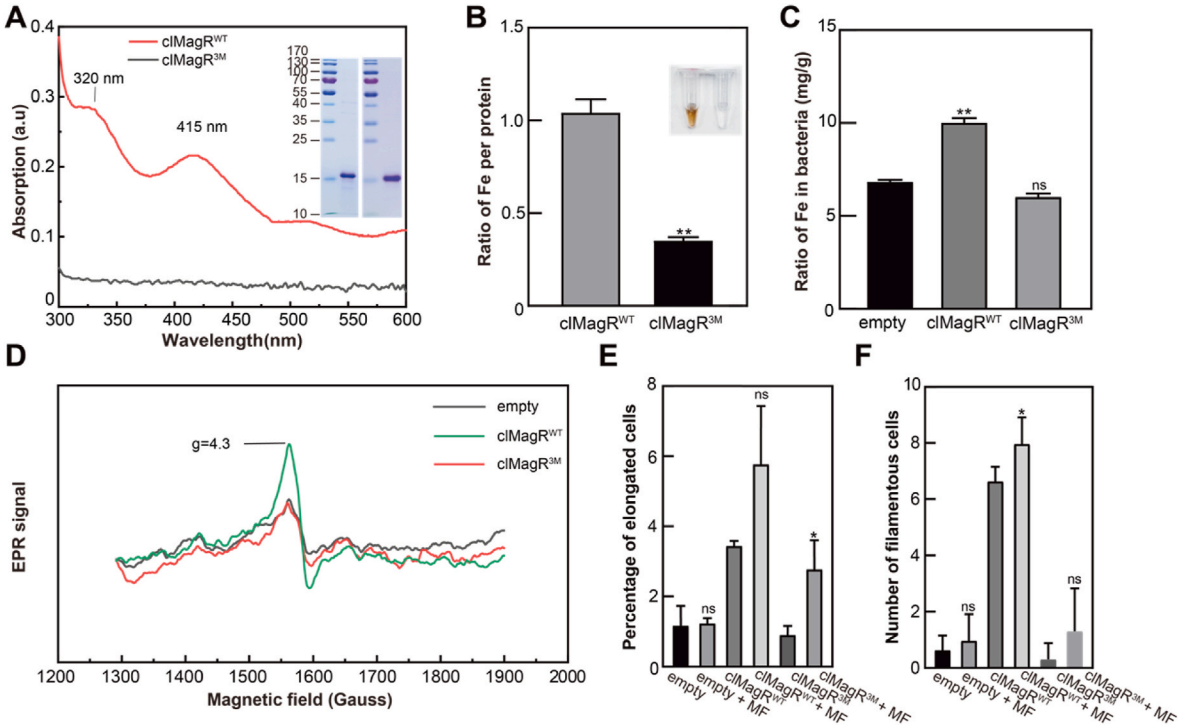

Fig. 5. Blocking the function of clMagR rescued the morphological change caused by clMagR^{WT} overexpression. (**A**) UV-Vis absorption spectrum of purified clMagR^{WT} (red line) and its loss-of-function mutant clMagR^{3M} (gray line). SDS-PAGE of purified proteins were shown as inserts. (**B**) Iron content of purified clMagR^{WT} protein (gray) and its mutant clMagR^{3M} protein (black) measured by Ferrozine assay. (**C**) Iron content of cells overexpressing clMagR^{WT}, clMagR^{3M} and none (empty) measured by Ferrozine assay. (**D**) The intracellular iron content of *E. coli* cells expressing clMagR^{WT} (green), clMagR^{3M} (red) and none (empty, black) measured by *in vivo* EPR. The amplitude of the EPR signal at g = 4.3 reflects the relative intracellular iron concentration in *E. coli* cells. (**E,F**) Percentage of elongated cells (**E**) and the number of filamentous cells (**F**) in *E. coli* overexpressing clMagR^{3M}, compared with cells overexpressing clMagR^{WT} and none (empty). Student's t-test: **, $p < 0.01$; ***, $p < 0.001$; ns, $p > 0.05$, "ns" indicate no significant differences. Error bars: SD of three experiments.

show increased ratio of morphological changed cells upon magnetic field treatment (Fig. 5EF), probably due to the innate magnetic property and the magnetic response of clMagR [23,24,27,35,44].

In all, our data suggested that the filamentous morphological change is associated with the overproduction of functional clMagR, which lead to the iron accumulation inside the cells, and the iron-sulfur cluster binding of clMagR is required.

4. Discussion

The morphology, refer to the size, shape, and structure of an organism, as well as the relationships of their constituent parts. Evolution shapes the morphology of organisms, but organisms also adapt their morphology to suit their environments. *E. coli* are bacteria found in the environment, food, and intestines of animals and human, and have been extensively studied as model systems. They are rod-shaped bacillus with regular dimensions, and many shape-related genes have been identified and used in morphology engineering.

E. coli is also the workhorse of molecular biology and has been instrumental in developing many fundamental concepts in biology. It is one of the most efficient expression hosts for recombinant proteins and widely used in scientific research and industries [45]. In most cases, recombinant expression of exogenous protein may change the growth rate of *E. coli*, but not dramatically change the shape of cells. We have been continuously noticed the filamentous shape change of *E. coli* cells during overexpression of clMagR in the lab for the last ten years. It is important to elucidate the underlying mechanism of this phenotype, which will expand our understanding of the morphology regulation of bacteria.

Comparative transcriptomic analysis strongly suggested that the change of iron metabolism and iron accumulation inside the cells could be the key to morphological change induced by overproduction of clMagR (Figs. 2 and 3), and this conception was supported by intracellular iron content measurements of cells expressing clMagR. To further test the hypothesis, we increased the iron content in cells by supplement the cells with ferric citrate in culture medium, or by overexpressing iron uptake related genes on cell membrane, and observed the similar filamentous morphological change of *E. coli* as well. Taking together, the data we presented here unambiguously proved that the accumulation of intracellular iron content by overproduction of clMagR led to the filamentous shape of bacteria (Fig. 6). It is worth pointing out that the increase of intracellular iron content upon clMagR expression, as shown in this study, is in agreement with previous studies as well [46,47].

Considering MagR is an ancient and extremely conserved protein throughout evolution from bacteria to human, not only as a putative magnetoreceptor, but also a key player in iron metabolism and iron-sulfur cluster assembly in both prokaryotes and eukaryotes. The filamentous morphology of bacteria cell caused by intracellular iron accumulation, or by the overproduction of MagR, may shed light on the morphology regulation of primitive cells. It also provides insight into novel approaches of morphology engineering in the future.

CRediT author statement

T. C. and C. X. conceived the idea and designed the study. M. W. carried out protein purification, fluorescence imaging, comparative transcriptomic analysis, site-directed mutagenesis, UV-Vis measurements, ferrozine assay and EPR experiments. C. H. helped with protein purification, and Y. T helped with EPR experiments and Ferrozine assay. X. Z. provided help in transcriptome data analysis. X. J. helped with the fluorescence imaging. X. Z., P. Z., Y. Z., Y. L. and J. Z. provided valuable suggestions on data analysis and experimental support. M.W. and T.C. and C.X. wrote the paper. X. Z. and P. Z. helped preparing the first draft of the manuscript. All authors read and approved the final version of the manuscript.

Funding

This study was supported by the National Natural Science Foundation of China (31640001 and T2350005 to C.X., U21A20148 to X.Z. and C.X.), Ministry of Science and Technology of China (2021ZD0140300 to C.X.); Presidential Foundation of Hefei Institutes of Physical Science, Chinese Academy of Sciences (Y96XC11131, E26CCG27, and E26CCD15 to C.X., E36CWGBR24B and E36CZG14132 to T.C.)

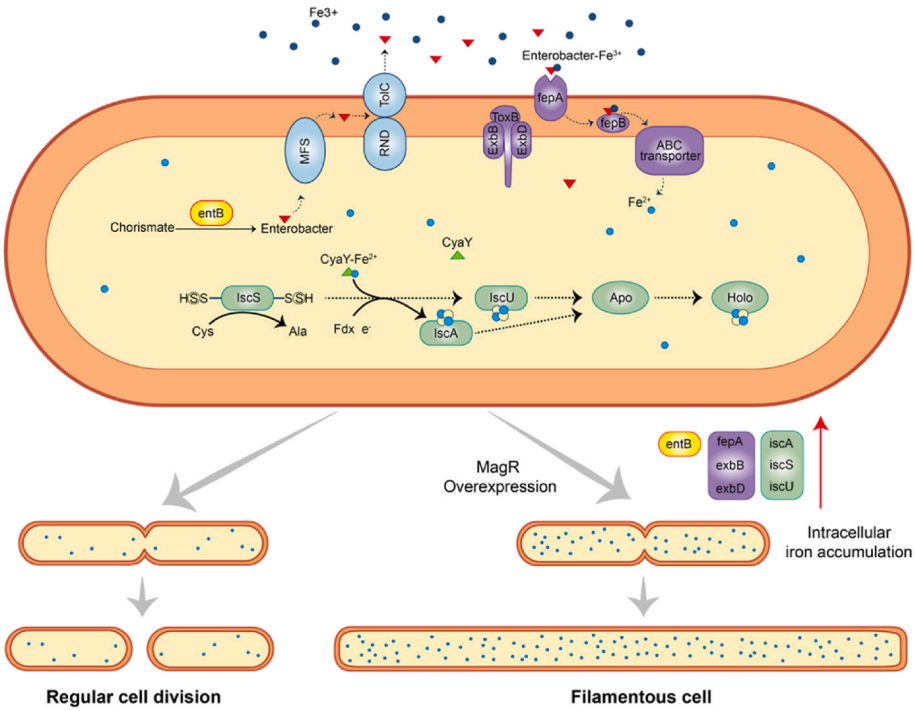

Fig. 6. Schmatic representation of filamentous morphological changes of *E. coli* cells caused by intracellular iron accumulation.

Declaration of competing interest

The authors declare that they have no known competing financial interests or personal relationships that could have appeared to influence the work reported in this paper.

Acknowledgements

We thank the Steady High Magnetic Field Facilities (High Magnetic Field Laboratory, CAS) for assistance with EPR measurements, and thanks to Dr. Wei Tong and Jinxing Li for their technical support.

Appendix A. Supplementary data

Supplementary data to this article can be found online at https://doi.org/10.1016/j.synbio.2024.04.009.

References

[1] Shiomi D, Mori H, Niki H. Genetic mechanism regulating bacterial cell shape and metabolism. Commun Integr Biol 2009;2(3):219–20.
[2] Khan F, Jeong GJ, Tabassum N, Mishra A, Kim YM. Filamentous morphology of bacterial pathogens: regulatory factors and control strategies. Appl Microbiol Biotechnol 2022;106(18):5835–62.
[3] Jiang XR, Chen GQ. Morphology engineering of bacteria for bio-production. Biotechnol Adv 2016;34(4):435–40.
[4] Jiang XR, Wang H, Shen R, Chen GQ. Engineering the bacterial shapes for enhanced inclusion bodies accumulation. Metab Eng 2015;29:227–37.
[5] Kruse T, Moller-Jensen J, Lobner-Olesen A, Gerdes K. Dysfunctional MreB inhibits chromosome segregation in *Escherichia coli*. EMBO J 2003;22(19):5283–92.
[6] Chen Y, Milam SL, Erickson HP. SulA inhibits assembly of FtsZ by a simple sequestration mechanism. Biochemistry 2012;51(14):3100–9.
[7] Andreini C, Bertini I, Rosato A. Metalloproteomes: a bioinformatic approach. Acc Chem Res 2009;42(10):1471–9.
[8] Foster AW, Young TR, Chivers PT, Robinson NJ. Protein metalation in biology. Curr Opin Chem Biol 2022;66:102095.
[9] Smethurst DGJ, Shcherbik N. Interchangeable utilization of metals: new perspectives on the impacts of metal ions employed in ancient and extant biomolecules. J Biol Chem 2021;297(6):101374.
[10] Chen AY, Adamek RN, Dick BL, Credille CV, Morrison CN, Cohen SM. Targeting metalloenzymes for therapeutic intervention. Chem Rev 2019;119(2):1323–455.
[11] Liu J, Chakraborty S, Hosseinzadeh P, Yu Y, Tian S, Petrik I, et al. Metalloproteins containing cytochrome, iron-sulfur, or copper redox centers. Chem Rev 2014;114(8):4366–469.
[12] Valentine JS. The inorganic-chemistry of biological processes - 2nd edition - hughes,Mn. J Am Chem Soc 1984;106(21):6463.
[13] Watanabe Y. Iron porphyrins .2.3. (Physical bioinorganic chemistry series), vol 1 and 2 - lever,Abp, gray,Hg. J Am Chem Soc 1983;105(16):5524–5.
[14] Bhagi-Damodaran A, Lu Y. The periodic table's impact on bioinorganic chemistry and biology's selective use of metal ions. Periodic Table Ii: Catal Mater Biol Med Appl 2019;182:153–73.
[15] Ahmed E, Holmstrom SJM. Siderophores in environmental research: roles and applications. Microb Biotechnol 2014;7(3):196–208.
[16] Oliveira F, Franca A, Cerca N. Staphylococcus epidermidis is largely dependent on iron availability to form biofilms. Int J Med Microbiol 2017;307(8):552–63.
[17] Chung PY. The emerging problems of Klebsiella pneumoniae infections: carbapenem resistance and biofilm formation. FEMS Microbiol Lett 2016;363(20).
[18] Andrews SC, Robinson AK, Rodriguez-Quinones F. Bacterial iron homeostasis. FEMS Microbiol Rev 2003;27(2–3):215–37.
[19] Esquilin-Lebron K, Dubrac S, Barras F, Boyd JM. Bacterial approaches for assembling iron-sulfur proteins. mBio 2021;12(6):e0242521.
[20] Fontecave M. Iron-sulfur clusters: ever-expanding roles. Nat Chem Biol 2006;2(4):171–4.
[21] Lill R. Function and biogenesis of iron-sulphur proteins. Nature 2009;460(7257):831–8.
[22] Beinert H. Iron-sulfur proteins: ancient structures, still full of surprises. J Biol Inorg Chem : JBIC : Publ Soc Biol Inorgan Chem 2000;5(1):2–15.
[23] Qin SY, Yin H, Yang C, Dou Y, Liu Z, Zhang P, et al. A magnetic protein biocompass. Nat Mater 2016;15(2):217–26.
[24] Zhou Y, Tong T, Wei M, Zhang P, Fei F, Zhou X, et al. Towards magnetism in pigeon MagR: iron- and iron-sulfur binding work indispensably and synergistically. Zool Res 2023;44(1):142–52.
[25] Yang P, Cai T, Zhang L, Yu D, Guo Z, Zhang Y, et al. A rationally designed building block of the putative magnetoreceptor MagR. Bioelectromagnetics 2022;43:317–26.
[26] Wang S, Zhang P, Fei F, Tong T, Zhou X, Zhou Y, et al. Unexpected divergence in magnetoreceptor MagR from robin and pigeon linked to two sequence variations. Zool Res 2024;45(1):69–78.
[27] Xie C. Searching for unity in diversity of animal magnetoreception: from biology to quantum mechanics and back. Innovation 2022;3(3):100229.
[28] Cao Y, Yan P. Role of atomic spin-mechanical coupling in the problem of a magnetic biocompass. Phys Rev 2018;97(4):042409.
[29] Xiao D-W, Hu W-H, Cai Y, Zhao N. Magnetic noise enabled biocompass. Phys Rev Lett 2020;124(12):128101.
[30] Chen Y, Jiang Y, Chen Y, Feng W, Liu G, Yu C, et al. Uncovering candidate genes responsive to salt stress in Salix matsudana (Koidz) by transcriptomic analysis. PLoS One 2020;15(8):e0236129.
[31] Li B, Dewey CN. RSEM: accurate transcript quantification from RNA-Seq data with or without a reference genome. BMC Bioinf 2011;12.
[32] Xie C, Mao X, Huang J, Ding Y, Wu J, Dong S, et al. Kobas 2.0: a web server for annotation and identification of enriched pathways and diseases. Nucleic Acids Res 2011;39(Web Server issue):W316–22.
[33] Chen C, Chen H, Zhang Y, Thomas HR, Frank MH, He Y, et al. TBtools: an integrative toolkit developed for interactive analyses of big biological data. Mol Plant 2020;13(8):1194–202.
[34] Guo Z, Xu S, Chen X, Wang C, Yang P, Qin S, et al. Modulation of MagR magnetic properties via iron-sulfur cluster binding. Sci Rep 2021;11(1):23941.
[35] Woodmansee AN, Imlay JA. Quantitation of intracellular free iron by electron paramagnetic resonance spectroscopy. Methods Enzymol 2002;349:3–9.
[36] Beall B, Lutkenhaus J. FtsZ in Bacillus subtilis is required for vegetative septation and for asymmetric septation during sporulation. Genes Dev 1991;5(3):447–55.
[37] Galli E, Gerdes K. FtsZ-ZapA-ZapB interactome of *Escherichia coli*. J Bacteriol 2012;194(2):292–302.
[38] Kramer J, Oezkaya O, Kuemmerli R. Bacterial siderophores in community and host interactions. Nat Rev Microbiol 2020;18(3):152–63.
[39] Santos JA, Alonso-Garcia N, Macedo-Ribeiro S, Pereira PJ. The unique regulation of iron-sulfur cluster biogenesis in a Gram-positive bacterium. Proc Natl Acad Sci U S A 2014;111(22):E2251–60.
[40] Im J, Lee J, Loffler FE. Interference of ferric ions with ferrous iron quantification using the ferrozine assay. J Microbiol Methods 2013;95(3):366–7.
[41] Landry AP, Cheng ZS, Ding HG. Iron binding activity is essential for the function of IscA in iron-sulphur cluster biogenesis. Dalton Trans 2013;42(9):3100–6.
[42] Gabriel GVD, Pitombo LM, Rosa LMT, Navarrete AA, Botero WG, do Carmo JB, et al. The environmental importance of iron speciation in soils: evaluation of classic methodologies. Environ Monit Assess 2021;193(2):63.
[43] Jacques JF, Jang S, Prevost K, Desnoyers G, Desmarais M, Imlay J, et al. RyhB small RNA modulates the free intracellular iron pool and is essential for normal growth during iron limitation in *Escherichia coli*. Mol Microbiol 2006;62(4):1181–90.
[44] Arai S, Shimizu R, Adachi M, Hirai M. Magnetic field effects on the structure and molecular behavior of pigeon iron–sulfur protein. Protein Sci 2022;31(6):e4313.
[45] Zhang ZX, Nong FT, Wang YZ, Yan CX, Gu Y, Song P, et al. Strategies for efficient production of recombinant proteins in *Escherichia coli*: alleviating the host burden and enhancing protein activity. Microb Cell Factories 2022;21(1):191.
[46] Li N, Xue L, Mai X, Wang P, Zhu C, Han X, et al. Transfection of clMagR/clCry4 imparts MR-T2 imaging contrast properties to living organisms (*E. coli*) in the presence of Fe^{3+} by endogenous formation of iron oxide nanoparticles. Front Mol Biosci 2023;10.
[47] Li N, Wang P, Xie Y, Wang B, Zhu C, Xue L, et al. Expression of clMagR/clCry4 protein in mBMSCs provides T(2)-contrast enhancement of MRI. Acta biomaterialia 2023;172:309–20.